It is also noteworthy that this is not an expensive operation, taking only a few hours on a minicomputer for the treatment of a thousand or more reflections. Except for the few origin-fixing phase sets, no multiple trials are necessary during the whole procedure. The figure-of-merit problem can normally be avoided.

The authors thank Drs D. Langs and H. King and Mr S. Potter for helpful discussions. This work was supported in part by NSF grants DMB-8610382 and CHE-8508724.

References

BERNSTEIN, F. C., KOETZLE, T. F., WILLIAMS, G. J. B., MEYER, E. F. JR, BRICE, M. D., ROGERS, J. R., KENNARD, O., SHIMANOUCHI, T. & TASUMI, M. (1977). *J. Mol. Biol.* **112**, 535-542.
GIACOVAZZO, C. (1983). *Acta Cryst.* A**39**, 585-592.
HAUPTMAN, H. (1982). *Acta Cryst.* A**38**, 632-641.
HAUPTMAN, H. & KARLE, J. (1956). *Acta Cryst.* **9**, 45-55.
OLTHOF, G. J. & SCHENK, H. (1982). *Acta Cryst.* A**38**, 117-122.
TIMKOVICH, R. & DICKERSON, R. E. (1973). *J. Mol. Biol.* **79**, 39-56.
TIMKOVICH, R. & DICKERSON, R. E. (1976). *J. Biol. Chem.* **251**, 4033-4046.
WOOLFSON, M. M. (1977). *Acta Cryst.* A**33**, 219-225.

Acta Cryst. (1991). A**47**, 490-497

Dynamical Treatment of the Splitting of HOLZ Lines from Dislocations in Silicon*

BY HUAMIN ZOU, XIFU YAO AND RENHUI WANG†

Department of Physics, Wuhan University, 430072 *Wuhan, People's Republic of China, and Beijing Laboratory of Electron Microscopy, Academia Sinica, PO Box* 2724, 100080 *Beijing, People's Republic of China*

(*Received* 25 *June* 1990; *accepted* 12 *March* 1991)

Abstract

The splitting of higher-order Laue-zone (HOLZ) lines of convergent-beam electron diffraction (CBED) due to the presence of dislocations in Si was investigated experimentally and theoretically. The parameters affecting the separation and relative positions of the fringes of split HOLZ lines were examined with experiments and/or computations. According to the results obtained, a method for identification of Burgers vector is discussed.

1. Introduction

The splitting of higher-order Laue-zone (HOLZ) lines in a convergent-beam electron diffraction (CBED) pattern from dislocations was first reported by Carpenter & Spence (1982). They found that a HOLZ line is split only if the value of $\mathbf{g}\cdot\mathbf{b}$ does not equal zero. By identifying lines that remain unsplit, implying $\mathbf{g}\cdot\mathbf{b}=0$, the direction of the Burgers vector of the dislocation can be determined. The intensity symmetry of Kikuchi bands reverses when the probe is moved from one side of the dislocation to the other, which can be used to identify the sense of $\mathbf{b}$. They also make a two-beam dynamical calculation to show that a line of the intensity minimum in the bright-field (BF) disc due to a HOLZ reflection can indeed split into two subsidiary minima due to the presence of a dislocation. Fung (1985) studied the HOLZ-line splitting from stacking faults and dislocations. He pointed out that the splitting and unsplitting of the reflections correspond to the visibility and invisibility of the defect in the kinematical theory of diffraction contrast of imperfect crystals. Preston & Cherns (1985) made a kinematical calculation of HOLZ rocking curves to show the splitting of HOLZ lines due to dislocations. When the whole strained area associated with a dislocation is illuminated by a defocus convergent beam, Cherns & Preston (1986) and Cherns, Kiely & Preston (1988) found that HOLZ deficiency lines close to the dislocation shadow image twist and split in the large-angle convergent-beam diffraction (LACBED) pattern (Tanaka pattern). Their simulation with kinematical approximation shows good qualitative agreement with the experiments. Tanaka, Terauchi & Kaneyama (1988) simulated LACBED patterns for dislocations with various characters (edge, screw and mixed) for different values of $\mathbf{g}\cdot\mathbf{b}$ and different depth of dislocation in the specimen with two-beam dynamical theory. They found that a HOLZ line generally splits into $n+1$ subsidiary fringes, where $n=\mathbf{g}\cdot\mathbf{b}$, around the intersection point of the HOLZ line and the shadow image of the dislocation and the HOLZ line twists in the opposite direction if the sign of $n=\mathbf{g}\cdot\mathbf{b}$ is changed. These results were successfully

* Project supported by the National Natural Science Foundation of China.

† To whom all correspondence should be addressed.

0108-7673/91/050490-08$03.00

used in determining the magnitude and direction of the Burgers vector **b** of a dislocation and also its sign (Niu, Wang & Lu, 1991). Several efforts have been put into the study of the distortion of zeroth-order Laue-zone (ZOLZ) patterns of LACBED due to the presence of dislocations (Carpenter & Spence, 1982; Wen, Wang & Lu, 1989; Lu, Wen, Zhang & Wang, 1990) and the HOLZ line splitting from stacking faults (Tanaka & Kaneyama, 1986; Tanaka, Terauchi & Kaneyama, 1988; Wang & Wen, 1989; Chou, Zhao & Ko, 1989).

Although there have been successes in the interpretation of the splitting of HOLZ lines using two-beam dynamical theory or even kinematical theory, it is necessary to do a many-beam dynamical calculation to confirm the correctness of these simplified treatments and to point out conditions under which these treatments hold. Many-beam dynamical treatment is absolutely necessary when two straight HOLZ lines are hybridized into two hyperbolic branches near their intersection point. In this case a convergent-beam diffraction pattern (CBP) cannot be obtained simply by superimposing patterns simulated with the two-beam calculation.

In this paper, firstly, we are going to describe our experimental results on the HOLZ-line splitting caused by dislocations in silicon (§ 2). Secondly, the calculated CBP of imperfect crystals, as well as of perfect crystals, are compared with the experimental patterns (§ 3). In § 4, the experimental conditions controlling the splitting of HOLZ lines are discussed. Finally the main points of this paper are summarized.

2. Experimental results

To introduce dislocations into a perfect silicon single crystal a crystal slice with surfaces parallel to the (111) plane was bent under three-point loading at 1170 K. Transmission electron microscopy (TEM) specimens were prepared from the deformed silicon by means of mechanical grinding and polishing and then by ion milling.

All microscopy examinations were conducted with a Philips EM 430 electron microscope equipped with a double-tilt goniometer at a nominal accelerating voltage of 150 kV. CBED experiments were carried out in nanoprobe mode. The probe size at focus was estimated to be 10 nm.

The line direction **u** and the Burgers vector **b** of a dislocation, which are defined according to the FS/RH perfect-crystal convention (*e.g.* Hirsch, Howie, Nicholson, Pashley & Whelan, 1977), were

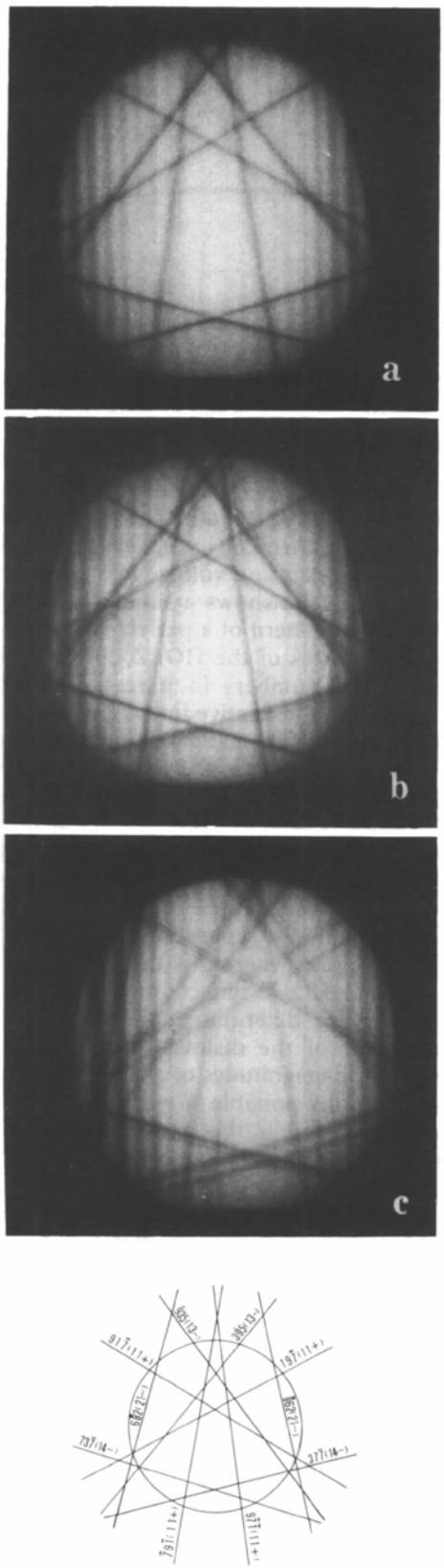

Fig. 1. BF discs from a [334] zone-axis pattern at a nominal voltage of 150 kV on moving closer to the dislocation with **b** equal to $\frac{1}{2}[101]$ and $\mathbf{u}/\!/[1\bar{8}9]$. (*a*), (*b*), (*c*) experimental patterns; (*d*) simulated HOLZ-line pattern with effective accelerating voltage of 149 kV.

Table 1. *Measurements of the angular separation of split HOLZ lines of Fig.* 1(*c*)

g			g . b	Separations (°)	Interplanar spacings (Å)
9	−7	−1	4	0·087	0·47443
−7	9	−1	−4	0·097	0·47443
3	−9	5	4	0·094	0·50636
6	−8	2	4	0·094	0·53247
1	9	−7	−3	0·073	0·47443
−8	6	2	−3		0·53247
−9	3	5	−2	0·063	0·50636
3	7	−7	−2	0·065	0·52495
9	1	−7	1	0·022	0·47443
7	3	−7	0	0·024	0·52495

determined to be $[1\bar{8}9]$ and $\frac{1}{2}[101]$ respectively by means of diffraction contrast and trace analysis.

Figs. 1(*a*), (*b*) and (*c*) show the splitting of HOLZ lines in a bright-field (BF) disc from a [334] zone-axis pattern on moving closer to a single dislocation. By matching the simulated HOLZ-line pattern with the experimental pattern taken in an area far from defects, the effective accelerating voltage was determined to be 149 kV. Fig. 1(*d*) shows a simulated [334] zone-axis HOLZ-line pattern of a perfect silicon crystal at 149 kV. The indices of the HOLZ lines are given in the figure. The numbers in parentheses after the indices represent the relative intensities of the HOLZ reflections in the kinematical approximation. The symbol, plus or minus, after each intensity value indicates that the HOLZ line in BF and the relevant HOLZ reflection lie on different sides of the center or on an identical side of the center, respectively.

Measurements of the angular separations between minima of split HOLZ lines in Fig. 1(*c*) are given in Table 1. The angular separation increases with the magnitude of $\mathbf{g} \cdot \mathbf{b}$, where $\mathbf{g}$ is the diffraction vector of the relevant HOLZ reflection. This phenomenon may be used for determining the direction of the Burgers vector of the dislocation by checking the sequence of the magnitudes of $\mathbf{g} \cdot \mathbf{b}$ for all the HOLZ lines and various possible $\mathbf{b}$ with the experimental results. The $73\bar{7}$ line in this case is clearly split even though the value of $\mathbf{g} \cdot \mathbf{b}$ equals zero. Since the type of dislocation examined in this work is a mixed dislocation, the dot product of the diffraction vector $\mathbf{g}$ and the displacement $\mathbf{R}$, $\mathbf{g} \cdot \mathbf{R}$, does not equal zero even if $\mathbf{g} \cdot \mathbf{b}$ equals zero. When the electron probe is moved a small distance away from the dislocation core, the $91\bar{7}$ lines with $\mathbf{g} \cdot \mathbf{b}$ equal to 1, as well as the $73\bar{7}$ line with $\mathbf{g} \cdot \mathbf{b}$ equal to zero, becomes unsplit as shown in Fig. 1(*b*). When the electron beam is moved further from the dislocation all the HOLZ lines become unsplit, as shown in Fig. 1(*a*). In addition, the interplanar spacings of relevant HOLZ reflections are given in Table 1. It is clear that the angular separation of split HOLZ lines is independent of the interplanar spacings.

In Fig. 1(*c*), the two intensity mimima for a split HOLZ line are nearly equal. In Fig. 1(*b*), however, it is seen that there is a darker line and a less-dark line for a split HOLZ line, which correspond to the major minimum and the subsidiary minimum of the intensity profile respectively. From an Ewald-sphere construction, one can see that if the HOLZ line and the corresponding HOLZ reflection lie on the same side relative to the center of the BF disc, the deviation parameter s on the side facing the center will be positive, whereas if the HOLZ line and the corresponding HOLZ reflection lie on different sides relative to the center, the s on the side facing the center will be negative. In short, the side on which $s > 0$ is always in the $-\mathbf{g}$ direction, where $\mathbf{g}$ is the diffraction vector of the relevant HOLZ reflection. In combination with the plus and minus symbol written in the parentheses of Fig. 1(*d*), we obtained the signs of s of the subsidiary minima of split HOLZ lines as shown in Table 2. Under the conditions of this experiment, when $\mathbf{g} \cdot \mathbf{b} > 0$ the subsidiary minimum is at the $s > 0$ side of the split HOLZ line, whereas if $\mathbf{g} \cdot \mathbf{b} < 0$ the less-dark line lies on the $s < 0$ side.

Table 2. *The relative positions of the subsidiary minima of split HOLZ lines in BF disc from Figs.* 1(*b*), 5(*a*) *and* 5(*b*)

g			g . b	Sign of s of subsidiary minima $-\mathbf{u} \times \mathbf{z}$ ($\mathbf{u} \times \mathbf{B}$) Experimental	$-\mathbf{u} \times \mathbf{z}$ ($\mathbf{u} \times \mathbf{B}$) Calculation	$\mathbf{u} \times \mathbf{z}$ ($-\mathbf{u} \times \mathbf{B}$) Calculation
9	−7	−1	4	+	+	
−7	9	−1	−4	−	−	+
3	−9	5	4	+	+	−
6	−8	2	4	+		
1	9	−7	−3	−	−	
−8	6	2	−3	−		
−9	3	5	−2	−	−	
3	7	−7	−2	−		
9	1	−7	1	0	0	
7	3	−7	0	0		

3. Computer simulation

The computer program was established on the basis of a wave-mechanical formulation of the many-beam dynamical theory developed by Jones, Rackham & Steeds (1977) using the scattering-matrix method (Hirsch *et al.*, 1977). The displacement vector $\mathbf{R}$ due to a general perfect dislocation was calculated with the formula developed for an infinite isotropic medium (see *e.g.* Hirsch *et al.*, 1977). The intensity distribution is displayed as a half-tone pattern (Head, Humble, Clarebrough, Morton & Forwood, 1973). To obtain the intensity distribution in a zone-axis CBP one needs to calculate the amplitudes along each incident-beam direction. The incident electrons travel in a cone outside the specimen with its vertex at the entrance surface of the specimen. At an exact Bragg angle, when the amplitudes of diffracted and transmitted beams are equal, the direction of energy flow is half way between the incident wave vector $\mathbf{k}$ and the diffracted wave vector $\mathbf{k} + \mathbf{g}$. With increasing deviation

from the Bragg angle the direction of energy flow reverts to that of the incident beam (Cowley, 1981). When an incident beam excites a HOLZ reflection, the energy flow will be in the direction which makes a small angle with the zone axis. In the case of a zone-axis pattern, *i.e.* the symmetrical case, the energy flow will travel in a cone with its axis parallel to the zone axis and a semi-vertex angle about 10^{-2} rad. Therefore, for the first-order approximation, it is reasonable to assume that the electron beam inside the specimen travels along the zone axis.

If not mentioned especially, all calculations in this paper have been conducted for a specimen thickness $t = 100$ nm and a depth of dislocation in the foil $z_0 = 0{\cdot}5t$.

As pointed out by Buxton (1976), including a large number of ZOLZ reflections will improve the computation accuracy of intensities for HOLZ reflections. Fig. 2(*a*) shows an intensity profile of the 791 HOLZ reflection calculated with the two-beam approximation. Fig. 2(*b*) is a profile of the same HOLZ reflection calculated with eight beams including seven ZOLZ reflections. It is seen that these two profiles show basically the same intensity distribution. Besides, if ZOLZ reflections are included in the computation, the ZOLZ fringes will appear in the computed CBP, which makes the pattern complicated and blurred. Secondly, the computation of the CBP from imperfect crystals with many beams is time consuming and the interaction between two HOLZ reflections when corresponding HOLZ lines intersect each other is more interesting. Hence, no ZOLZ reflections except 000 are included in the following calculation.

Fig. 3 shows the computed [334] CBP from a perfect Si crystal. Nine beams, *i.e.* 000, $\bar{7}9\bar{1}$, $9\bar{7}\bar{1}$, $3\bar{9}5$, $\bar{9}35$, $19\bar{7}$, $91\bar{7}$, $37\bar{7}$ and $73\bar{7}$, are included in the calculated pattern. From comparison of this pattern with the experimental picture in Fig. 1(*a*), which contains unsplit HOLZ lines, we can see that they agree very well in two aspects: the relative positions of HOLZ lines and the hyperbolic splitting in the crossover of $73\bar{7}$ and $37\bar{7}$ HOLZ lines as indicated by an arrow in these two pictures.

Fig. 4 shows the calculated [334] CBP when the electron probe position is 30 nm from the dislocation core in the direction of $\mathbf{u}\times\mathbf{z}$, where $\mathbf{u}$ is the direction of the dislocation line and $\mathbf{z}$ is the zone axis. The good agreement between the calculated pattern and the experimental Fig. 1(*c*) can be seen from the relative positions and the separations between major and subsidiary intensity minima of the split HOLZ lines involved in both figures. The intensities of subsidiary minima do not match the experimental picture very well, which may be due to the limited number of ZOLZ electron beams involved in the calculation.

Fig. 5(*a*) shows a simulated pattern when the electron probe is placed on the side pointed to by the vector $-\mathbf{u}\times\mathbf{z}$ and 70 nm from the dislocation core. By comparison with Fig. 1(*b*), it is seen that not only the positions of split HOLZ lines but also the relative positions of subsidiary minima with respect to the major minima in the computed picture match Fig. 1(*b*) quite well. The separation of the split $91\bar{7}$ line in this case is so small that the 917 line appears as if

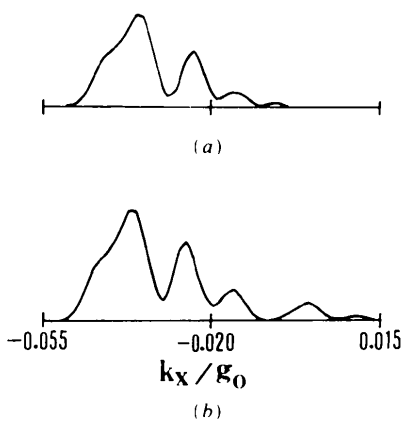

Fig. 2. Intensity profiles of $\bar{7}9\bar{1}$ HOLZ reflection calculated with two beams (*a*) and with eight beams including seven ZOLZ reflections (*b*). The direction of the incident electron beam changes with k_x along g_0, the horizontal component of the diffraction vector $\bar{7}9\bar{1}$ and $k_y = 0$, where k_x and k_y are the components of k_0, the horizontal component of wave vector $\mathbf{k}^{(j)}$. Thickness of specimen = 100 nm, effective accelerating voltage = 149 kV and the ratio of the imaginary part U'_g to the real part U_g of the Fourier components of the crystal potential is assumed to be 0·1. The electron probe is 40 nm away from the dislocation ($\mathbf{b} = \frac{1}{2}[101]$, $\mathbf{u} = [1\bar{8}9]$) on the side pointed to by $-\mathbf{u}\times\mathbf{z}$.

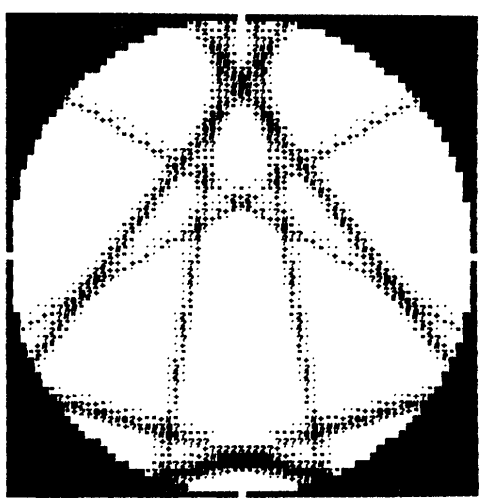

Fig. 3. Calculated central disc of the [334] zone-axis pattern from a perfect crystal of Si. Nine beams, *i.e.* 000, $\bar{7}9\bar{1}$, $9\bar{7}\bar{1}$, $3\bar{9}5$, $\bar{9}35$, $19\bar{7}$, $91\bar{7}$, $37\bar{7}$ and $73\bar{7}$, are included in the calculation. Effective accelerating voltage 149 kV, lattice parameter $a = 0{\cdot}54\,301$ nm, semi-angle of convergence 0·354° ($k_x/g_{220} = 0{\cdot}4$) and $U'_g = 0{\cdot}1\,U_g$.

unsplit in the computed pattern and this agrees with that shown in Fig. 1(*b*).

With the electron probe placed on the side pointed to by the vector $\mathbf{u}\times\mathbf{z}$ and 70 nm from the real dislocation line, *i.e.* on the opposite side to that of Fig. 5(*a*) symmetrically about the dislocation line, the calculated pattern is shown in Fig. 5(*b*). From comparison of Figs. 5(*a*) and (*b*), it is found that the shifts of HOLZ lines and the displacements of less-dark lines with respect to darker lines in the two patterns are roughly in opposite directions. This phenomenon may be a reflection of the fact that the atomic planes in the two sides of the dislocation tilt roughly, not exactly, in opposite directions. The relative positions of the subsidiary minima of split HOLZ lines in the computed patterns, Figs. 5(*a*), (*b*), are given in columns 4 and 5 of Table 2, which follow the same rule as in the experimental pattern. When the electron probe is focused on the $-\mathbf{u}\times\mathbf{z}$ side (*i.e.* $\mathbf{u}\times\mathbf{B}$ side with $\mathbf{B}$ the direction of the incident beam, $\mathbf{B}=-\mathbf{z}$) of the dislocation the subsidiary minimum lines on the $s>0$ side for $\mathbf{g}\cdot\mathbf{b}>0$ and on the $s<0$ side for $\mathbf{g}\cdot\mathbf{b}<0$, which leads to a relation $(\mathbf{g}\cdot\mathbf{b})s_g>0$. Column 5 shows that if the electron probe is on the $\mathbf{u}\times\mathbf{z}$ (*i.e.* $-\mathbf{u}\times\mathbf{B}$) side of the dislocation the subsidiary minimum lies on the $s<0$ side for $\mathbf{g}\cdot\mathbf{b}>0$ and on the $s>0$ side for $\mathbf{g}\cdot\mathbf{b}<0$, which means $(\mathbf{g}\cdot\mathbf{b})\mathbf{s}_g<0$. This phenomenon may be used to identify the sense of the Burgers vector of a dislocation by taking CBP at both sides of the dislocation. It is interesting to notice that this relationship is similar to that of the diffraction contrast image of a dislocation (Hirsch *et al.*, 1977), namely, the image of the dislocation is on the side pointed to by the vector $\mathbf{u}\times\mathbf{B}$ (or $-\mathbf{u}\times\mathbf{B}$) from the dislocation line when $(\mathbf{g}\cdot\mathbf{b})\mathbf{s}_g>0$ [or $(\mathbf{g}\cdot\mathbf{b})\mathbf{s}_g<0$]. This can be qualitatively explained as follows. In the case of diffraction contrast imaging, for instance, if $(\mathbf{g}\cdot\mathbf{b})\mathbf{s}_g>0$ and $\mathbf{g}\cdot\mathbf{b}>0$, the amplitude of the outgoing diffraction beam at the exit surface of a crystal is very small everywhere (since $s_g>0$) except that somewhere on the side pointed to by $\mathbf{u}\times\mathbf{B}$ near the dislocation the deviation $\mathbf{s}_g$ becomes zero so that the amplitude of the diffraction beam is large. Then the image of the

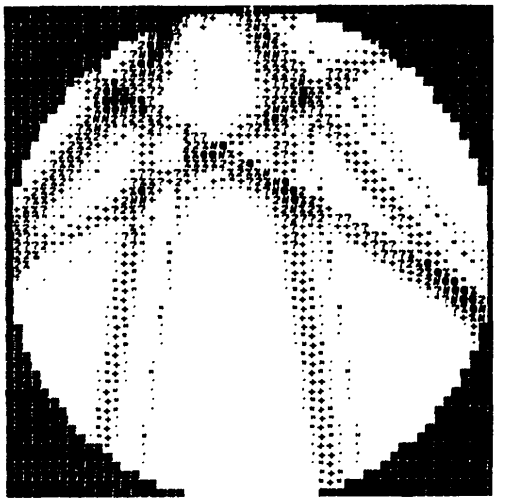

(*a*)

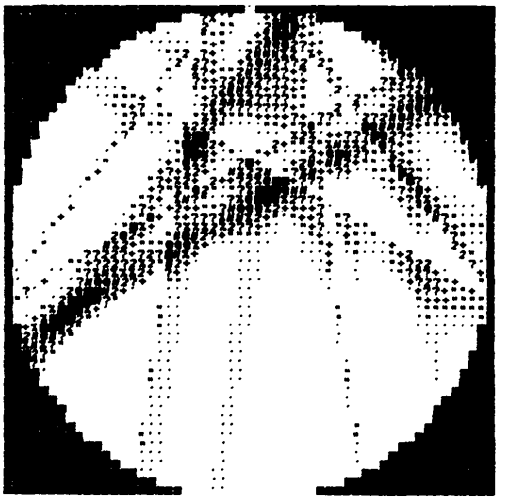

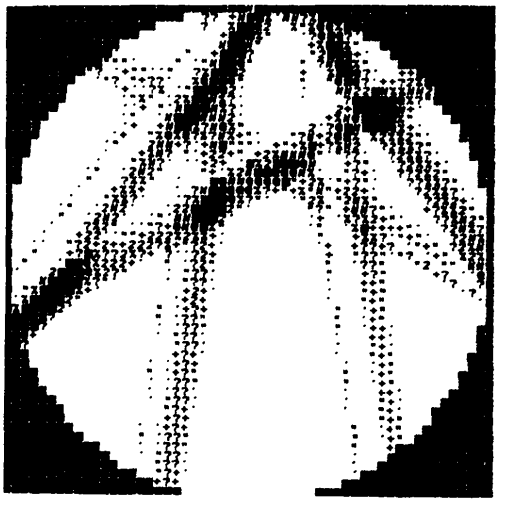

(*b*)

Fig. 4. Dynamical simulation of the central part of the BF image of the [334] zone-axis pattern when the electron probe is 30 nm from the real line of the dislocation with $\mathbf{b}=\frac{1}{2}[101]$ and $\mathbf{u}=[1\bar{8}9]$ at 149 kV. Seven beams, 000, $\bar{7}9\bar{1}$, $9\bar{7}\bar{1}$, $3\bar{9}5$, $\bar{9}35$, $19\bar{7}$ and $91\bar{7}$, are included in the computation. The semi-angle of convergence is 0·22° ($k_x/g_{220}=0{\cdot}25$). Other parameters for the computation are the same as for Fig. 3.

Fig. 5. Simulation of the central part of the BF disc of the [334] zone-axis pattern when the electron probe is 70 nm away from the real dislocation line in the direction of (*a*) $-\mathbf{u}\times\mathbf{z}$ (*i.e.* $\mathbf{u}\times\mathbf{B}$) and (*b*) $\mathbf{u}\times\mathbf{z}$ (*i.e.* $-\mathbf{u}\times\mathbf{B}$). Other parameters used in the calculations are the same as those in Fig. 4.

dislocation, a dark line, forms on the $\mathbf{u}\times\mathbf{B}$ side of the real dislocation line. Similarly, in the case of CBED, as an example, we may discuss the situation when the electron probe is positioned on the $\mathbf{u}\times\mathbf{B}$ side of the dislocation with $\mathbf{g}\cdot\mathbf{b}>0$. If an electron beam satisfies the Bragg law for most of a given atomic-plane family, the distortion will make the atomic plane on this side near the dislocation tilt in the $-\mathbf{s}$ direction. Another incident beam which makes the part of the crystal nearest the dislocation satisfy the Bragg condition will cause a positive deviation parameter for the remaining part of the crystal in the column. Because the part of the crystal affected by the dislocation is usually a small fraction of the whole plane, a less-dark line, *i.e.* the subsidiary minimum, forms in the $+\mathbf{s}$ side of the darker line (the major minimum). From this simple analysis, it is seen that the separation is related to the degree of distortion of atomic planes in the vicinity of the dislocation, which is also confirmed by the experimental results that the separations of split HOLZ lines in Fig. 1(*c*) are greater than those in Fig. 1(*b*) and the former is produced when the probe is closer to the dislocation core, *i.e.* the area with stronger distortion, than that for the latter.

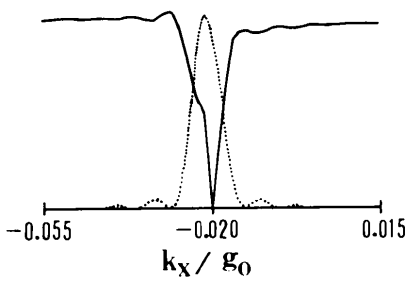

Fig. 6. Intensity profiles of $\bar{7}9\bar{1}$ HOLZ line in BF (solid line) and relevant HOLZ reflection (dotted line) for a perfect Si foil with thickness of 100 nm, effective accelerating voltage 149 kV and $U'_g = 0{\cdot}1\,U_g$. In order to demonstrate the intensity distribution of the HOLZ reflection better, the intensity scale for the HOLZ reflection is different from that for HOLZ line.

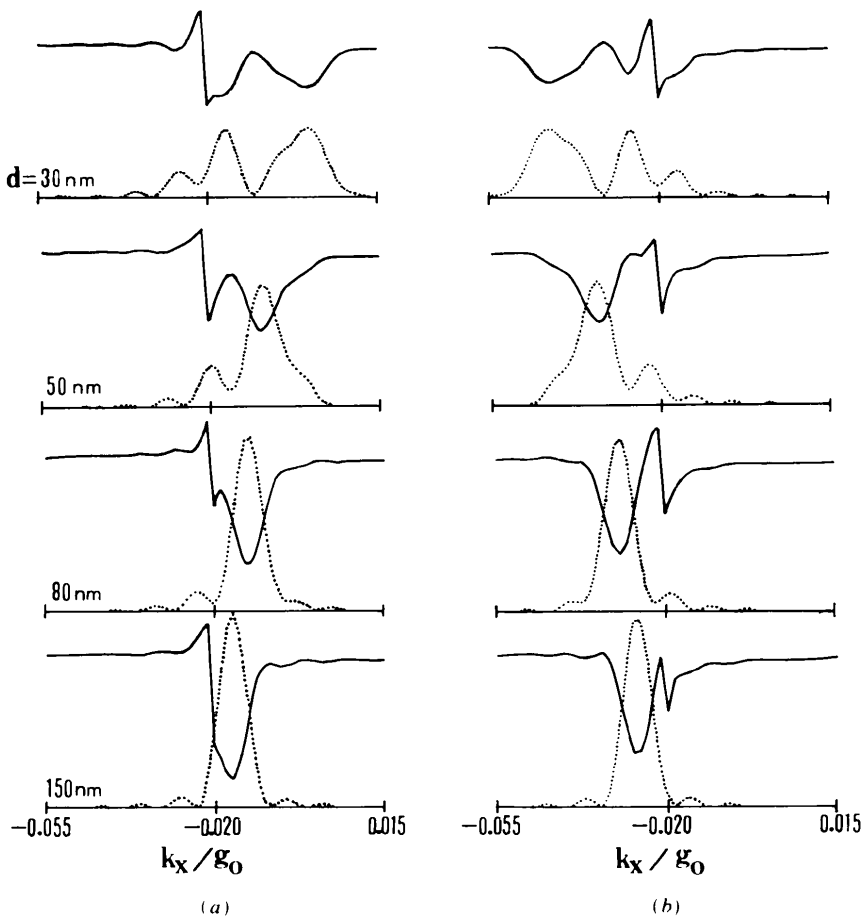

Fig. 7. Changes in intensity profiles of the 791 HOLZ line with increase in distance *d*. The dislocation with $\mathbf{b}=\frac{1}{2}[101]$, $\mathbf{u}=[1\bar{8}9]$ is in the middle of the column and the thickness is 100 nm. The distance between the electron probe and the real dislocation line changes from 30 to 150 nm as indicated in the figures. The electron probe is focused on the side of the dislocation pointed to by vector $\mathbf{u}\times\mathbf{z}$ (*a*) or $-\mathbf{u}\times\mathbf{z}$ (*b*). $U'_g = 0{\cdot}1\,U_g$.

4. Experimental conditions affecting the HOLZ line splitting

Two-beam dynamical calculations were performed in order to study the effect of the distance d between the electron probe and the dislocation line, the thickness t of the sample and the depth z_0 of the dislocation in the sample on the splitting of HOLZ lines. Fig. 6 shows intensity profiles of the $\bar{7}9\bar{1}$ HOLZ line in BF and of the $\bar{7}9\bar{1}$ HOLZ reflection, which acts as a reference for studying the splitting and shifting of HOLZ lines due to the presence of a dislocation.

4.1. *Distance between the electron probe and the dislocation core*

Fig. 7 shows the intensity profiles of the $\bar{7}9\bar{1}$ HOLZ line in BF and the corresponding HOLZ reflection for different distances d from 30 to 150 nm. The electron probe is focused on the side of the dislocation pointed to by $\mathbf{u}\times\mathbf{z}$ (*i.e.* $-\mathbf{u}\times\mathbf{B}$) (*a*) or by $-\mathbf{u}\times\mathbf{z}$ ($\mathbf{u}\times\mathbf{B}$) (*b*). Since $\mathbf{g}\cdot\mathbf{b}<0$ in the present case, the less-dark line in BF lies on the $s>0$ side for case (*a*) and on the $s<0$ side for case (*b*), which obeys the rule mentioned in § 3. The separation decreases with increasing distance from the real dislocation line. By comparison with Fig. 6, it is seen that the shift of the darker line in BF with respect to the position for a perfect crystal also decreases with the increase in the distance. Moreover, for Fig. 7(*a*), when the distance reaches 150 nm, the HOLZ line becomes unsplit, but the displacement of the HOLZ line is still appreciable, which may cause HOLZ-line patterns to be distorted. This indicates that the strain produced by a dislocation changes from nonuniform to uniform and hence the HOLZ line changes from split to unsplit but shifted as the distance from the dislocation increases.

4.2. *Depth*

The influence of the depth z_0 at which the dislocation lies under the top surface of the sample on the splitting of the HOLZ lines is shown in Fig. 8. The separation of the split HOLZ line decreases and the less-dark line gets stronger as the dislocation line is closer to the bottom surface. When the dislocation lies in the middle of the specimen, the splitting of the HOLZ line is seen best.

4.3. *Thickness of sample*

The intensity profiles of a split $\bar{7}9\bar{1}$ line for different thicknesses t from 80 to 200 nm are shown in Fig. 9. As the thickness of the specimen increases, in addition to the decrease in intensity due to absorption, the number of fringes in the split HOLZ line increases and the separation of the main fringes gets smaller. In order to observe splitting of HOLZ lines better, thin specimens are preferred.

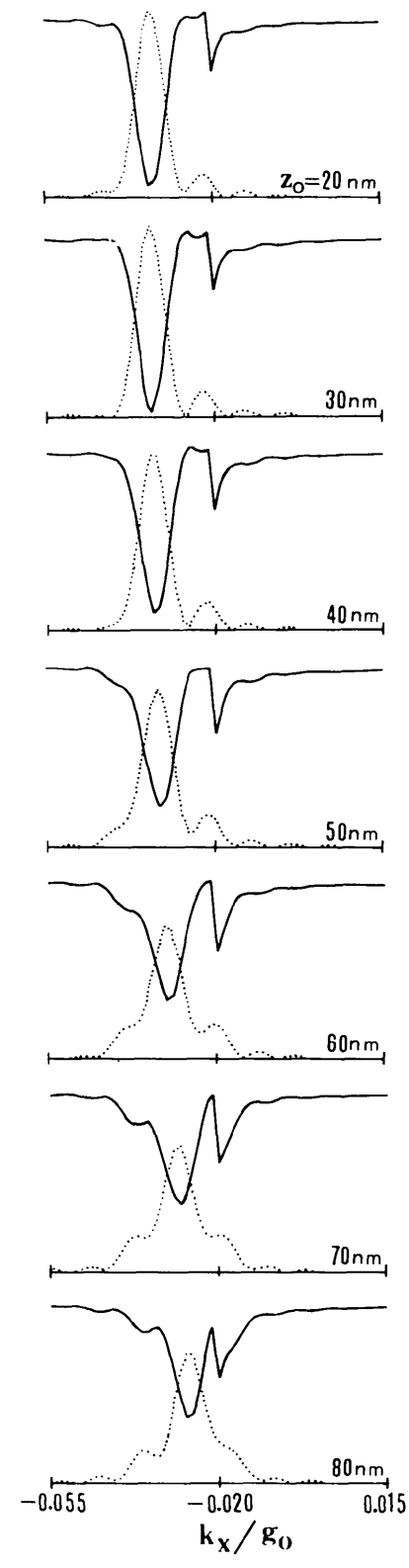

Fig. 8. Influence of the depth z_0 of the dislocation under the top surface on the splitting of the $\bar{7}9\bar{1}$ HOLZ line. The dislocation with $\mathbf{b}=\frac{1}{2}[101]$ and $\mathbf{u}=[1\bar{8}9]$ lies on the side pointed to by vector $-\mathbf{u}\times\mathbf{z}$ with $d=60$ nm, $t=100$ nm, $U_g'/U_g=0{\cdot}05$.

5. Summary

The splitting of HOLZ lines due to the presence of a mixed dislocation in Si is studied both experimentally and theoretically in the present work. The simulations of HOLZ-line splitting due to a dislocation, based on many-beam dynamical diffraction theory including the column approximation, agree well with the experimental results. The main points are as follows.

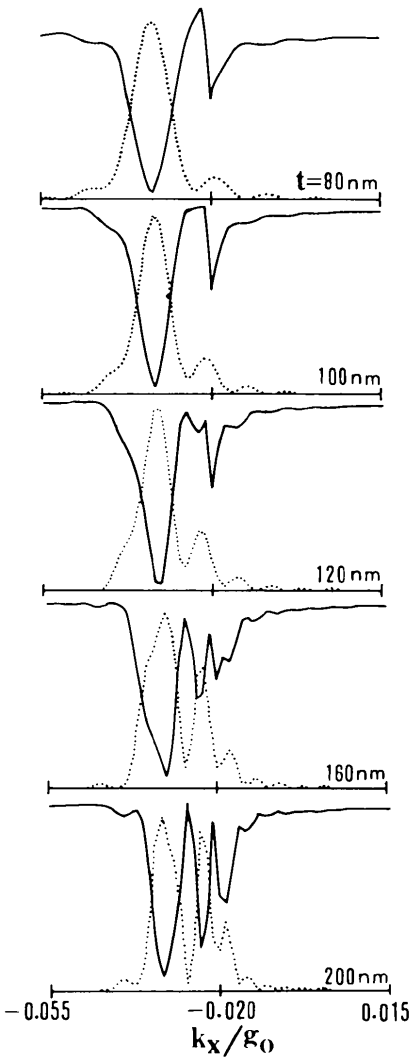

Fig. 9. Intensity profiles of the $\bar{7}9\bar{1}$ HOLZ line with electron probe 60 nm from the real dislocation line. The dislocation is at the middle of the specimen. The thickness, t, of the specimen changes from 80 to 200 nm as indicated in the figures. $U'_g = 0{\cdot}05\,U_g$. The intensity scales for different thicknesses as well as for the HOLZ line in BF and for HOLZ reflection are different.

(1) The separation of HOLZ lines increases with the magnitude of $\mathbf{g}\,.\,\mathbf{b}$.

(2) The splitting of HOLZ lines with $\mathbf{g}\,.\,\mathbf{b} = 0$ but $\mathbf{g}\,.\,\mathbf{R} \neq 0$ is observed, which corresponds to the residual contrast in imaging experiments.

(3) When the electron probe is positioned on the side pointed to by the vector $\mathbf{u} \times \mathbf{B}$ near the dislocation line, the subsidiary minimum in BF lies on the $s > 0$ side (for $\mathbf{g}\,.\,\mathbf{b} > 0$) or $s < 0$ side (for $\mathbf{g}\,.\,\mathbf{b} < 0$) and *vice versa*.

(4) The direction of the Burgers vector can be determined by checking the sequence of magnitudes of $\mathbf{g}\,.\,\mathbf{b}$ for all the observed HOLZ lines and various possible $\mathbf{b}$ with the experimental results. The sense of $\mathbf{b}$ may be identified by examining the relative positions of the subsidiary intensity minima of the split HOLZ lines.

(5) The shift and separation of the split HOLZ lines can be influenced by the depth z_0 at which the dislocation lies and the thickness t of the specimen as well as by the distance d between the electron probe and the real dislocation line.

References

BUXTON, B. F. (1976). *Proc. R. Soc. London Ser. A*, **350**, 335-361.

CARPENTER, R. W. & SPENCE, J. C. H. (1982). *Acta Cryst.* A**38**, 55-61.

CHERNS, D., KIELY, C. J. & PRESTON, A. R. (1988). *Ultramicroscopy*, **24**, 355-369.

CHERNS, D. & PRESTON, A. R. (1986). Proc. XIth Int. Congr. Electron Microscopy, Kyoto, Japan, pp. 721-722.

CHOU, C. T., ZHAO, L. J. & KO, T. (1989). *Philos. Mag.* A**59**, 1221-1243.

COWLEY, J. M. (1981). *Diffraction Physics*. Amsterdam: North-Holland.

FUNG, K. K. (1985). *Ultramicroscopy*, **17**, 81-86.

HEAD, A. K., HUMBLE, P., CLAREBROUGH, L. M., MORTON, A. J. & FORWOOD, C. T. (1973). *Computed Electron Micrographs and Defect Identification*. Amsterdam: North-Holland.

HIRSCH, P., HOWIE, A., NICHOLSON, R. B., PASHLEY, D. W. & WHELAN, M. J. (1977). *Electron Microscopy of Thin Crystals*. Huntington, New York: Robert E. Krieger.

JONES, P. M., RACKHAM, G. M. & STEEDS, J. W. (1977). *Proc. R. Soc. London Ser. A*, **354**, 197-222.

LU, G., WEN, J. G., ZHANG, W. & WANG, R. (1990). *Acta Cryst.* A**46**, 103-112.

NIU, F., WANG, R. & LU, G. (1991). *Acta Cryst.* A**47**, 36-39.

PRESTON, A. R. & CHERNS, D. (1985). In *Electron Microscopy and Analysis* 1985. *Inst. Phys. Conf. Ser. No.* 78, edited by G. J. TATLOCK, pp. 41-44. Bristol; Boston: Adam Hilger.

TANAKA, M. & KANEYAMA, T. (1986). Proc. XIth Int. Congr. Electron Microscopy, Kyoto, Japan, pp. 203-206.

TANAKA, M., TERAUCHI, M. & KANEYAMA, T. (1988). *Convergent-Beam Electron Diffraction* II. Tokyo: JEOL-Maruzen.

WANG, R. & WEN, J. (1989). *Acta Cryst.* A**45**, 428-431.

WEN, J., WANG, R. & LU, G. (1989). *Acta Cryst.* A**45**, 422-427.